Complex Three-Dimensional Tungsten Oxide Nanowire Networks: Controllable Synthesis and Growth Mechanism

ARTICLE *in* CRYSTENGCOMM · NOVEMBER 2014

Impact Factor: 4.03 · DOI: 10.1039/C4CE01715C

8 AUTHORS, INCLUDING:

Jian Yi Luo

Wuyi University

29 PUBLICATIONS **230** CITATIONS

SEE PROFILE

Q.G. Zeng

University of Science and Technology of Ch…

28 PUBLICATIONS **254** CITATIONS

SEE PROFILE

CrystEngComm

PAPER

Cite this: *CrystEngComm*, 2015, **17**, 889

Complex three-dimensional tungsten oxide nanowire networks: controllable synthesis and growth mechanism†

Jian Yi Luo,*[a] Feng Chen,[b] Zhi Cao,[a] Wen Hao Zheng,[a] Huan Cong Liu,[a] Yu Dong Li,[a] Guo Tao Yang[a] and Qing Guang Zeng*[a]

Received 19th August 2014,
Accepted 19th November 2014

DOI: 10.1039/c4ce01715c

www.rsc.org/crystengcomm

Tungsten oxide nanorods, nanowires, and three-dimensional (3D) nanowire networks have been synthesized just by controlling an oxygen flow rate which was introduced in thermal evaporation. X-ray diffraction (XRD) results show that the crystal structures of the nanostructural film are indexed to WO_2, $W_{18}O_{49}$, and WO_3 phases in sequence with the increase in the oxygen flow rate. High-resolution scanning electron microscopy, transmission electron microscopy, and XRD spectroscopy are applied to investigate the formation process of 3D nanowire networks, and the results indicate that the nanorods grow into nanotrees, and then the nanowire networks grow along a preferred orientation from the bottom to the top with the increase in evaporation time. The growth mechanism for complex 3D-WO_3 nanowire networks is also discussed in detail.

Introduction

Tungsten oxide has been widely investigated as a new functional material, owing to its promising applications in chromic devices (such as electrochromic displays, gasochromic smart windows, and photochromic glass),[1–4] gas sensors,[5,6] photocatalytic technologies[7–9] and supercapacitors.[10] Recently, one dimensional tungsten oxide nanostructures (nanowires, nanotubes, and nanorods) have been demonstrated to be a good candidate for the applications mentioned above by our group[11,12] and some other groups.[13–16] However, when these nanostructures are used as a functional layer in the actual electronic and optoelectronic devices, the performance of these nanostructures is usually unstable, due to the poor electronic connection between nanostructures. For instance, when a current passes through the nanowire-network structure in the nanowire film, the carriers (*e.g.*, electrons) need to tunnel through a large number of nano-junctions between nanowires.[17,18] These nano-junctions are often formed by physical contact between nanowires, and will be prone to poor contact when the environmental conditions (such as temperature and humidity) change. If single crystalline three-dimensional (3D) nanowire networks can be directly synthesized by a crystal growth method, there is no nano-junction in a single crystalline nanowire network in which the intersections had been formed in the crystal growth process, avoiding the poor contact of nano-junctions. Thus, the assembly of one dimensional nanowires into complex functional devices by direct growth through branching is still challenging work, although some breakthrough studies had been made by Lieber's group and other groups.[19–24]

Some successful examples in the synthesis of 3D tungsten oxide nanostructures include micro-tree structures,[25] 3D nanowire networks with a cubic phase,[26] and the 3D hierarchical structure of nanowires on carbon microfibers.[27] In this paper, more complex 3D-WO_3 nanowire networks have been synthesized in a one-step high temperature, catalyst free, thermal evaporation deposition process. These complex 3D-WO_3 nanowire networks have a special hierarchical structure, which is composed of nanorods, nanotrees and nanowire networks from the bottom to the top, and the whole complex structure is single crystalline. The controllable synthesis conditions and the crystal growth process for complex 3D-WO_3 nanowire networks have also been investigated in detail.

Experimental section

Materials synthesis

Tungsten oxide nanowires were prepared by a one-step high temperature, catalyst free, thermal evaporation deposition process. As shown in Fig. 1(a), the experimental setup consisted of a vacuum chamber (Φ, 300 mm × 400 mm),

[a] *School of Applied Physics and Materials, Wuyi University, Jiangmen, Guangdong, 529020, PR China. E-mail: luojiany@mail3.sysu.edu.cn, zengqg@mail.ustc.edu.cn*
[b] *School of Chemical and Environment Engineering, Wuyi University, Jiangmen, Guangdong, 529020, PR China*

† Electronic supplementary information (ESI) available. See DOI: 10.1039/c4ce01715c

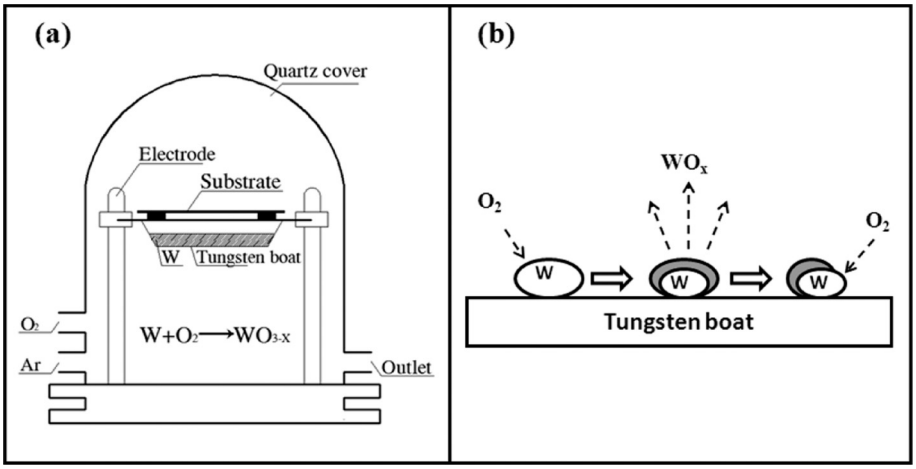

Fig. 1 Illustrations of the (a) experimental setup and (b) chemical reaction process for the formation of tungsten oxide vapor.

two copper electrodes, a rotary pump system, and a gas controlling system. A tungsten boat (120 mm × 20 mm × 0.3 mm) was placed and fixed on the copper electrodes. High purity tungsten powder (0.5 g, 99.95%) was spread out on the bottom of the tungsten boat as a source. Silicon or quartz substrates were placed above the boat with one side facing the boat, and ceramic strips were used as spacers between the substrates and the boat. When the vacuum chamber was first evacuated down to about 0.1 Pa, mixed gases of high purity argon gas and oxygen gas (both purities were 99.999%) were introduced into the chamber. The flow rate of argon gas was fixed at 100 standard cubic centimeters per minute (sccm), while the flow rate of oxygen gas was changed in the range of 0–2.0 sccm. The tungsten boat was then heated to 1100 °C and held at the peak temperature for a period of time (1–20 min). After introducing the flow of mixed gases, the gas pressure in the vacuum chamber remained stable at about 10 Pa. The involved chemical reaction process responsible for the formation of tungsten oxide vapor during the evaporation was proposed as shown in Fig. 1(b). The surface layer of tungsten particles could be oxidized into tungsten oxide (WO_x, $2.0 \leq x \leq 3.0$) at relatively low temperature (*e.g.*, 500 °C),[28] and then the solid tungsten oxide could be evaporated into WO_x vapor at a peak temperature of 1100 °C during the evaporation deposition process. The newly exposed tungsten on the particle surface could also be oxidized into tungsten oxide and then become tungsten oxide vapor, making the particle smaller in size.

Characterization

The morphologies, chemical compositions, and the structures of the prepared products were characterized by field emission scanning electron microscopy (SEM, Nova Nano SEM 432), X-ray diffraction spectroscopy (XRD, X'pert Pro with Cu Kα radiation), and high-resolution transmission electron microscopy (TEM, FEI Tecnai GZ F30 at 300 kV). In order to confirm whether the tungsten powder was oxidized in air or not before thermal evaporation deposition, the crystal structure of the tungsten powder was analyzed by XRD.

Results and discussion

The morphologies of tungsten oxide nanowires were very sensitive to the oxygen gas flow rates which had been introduced into the vacuum chamber during the evaporation deposition process. As displayed in Fig. 2, the typical SEM images show that when the high purity oxygen gas was not introduced into the vacuum chamber, the synthesized nanowires had relatively short length (about 1.0 μm) and large average diameter (larger than 200 nm), and these could be denoted as nanorods. As the oxygen gas flow rates increased from 0 to 1.5 sccm,

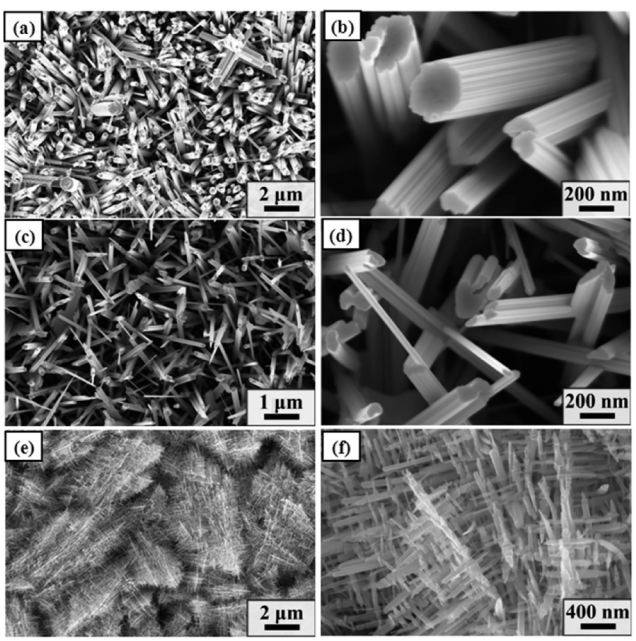

Fig. 2 Top-view SEM images of the products prepared at oxygen flow rates of (a, b) 0 sccm, (c, d) 1.0 sccm, and (e, f) 1.5 sccm.

the average diameter of the nanowires obviously decreased to several tens of nanometers, and the morphologies also changed from quasi one-dimensional nanowires to three-dimensional (3D) nanowire networks. Especially, when the oxygen flow rate reached 1.5 sccm, a high yield of three-dimensional (3D) nanowire networks was uniformly obtained on the substrate as shown in the low-magnification SEM image in Fig. 2(e). The high-magnification SEM image in Fig. 2(f) clearly demonstrates that the 3D nanowire networks were constructed of nanowires with diameters ranging from 10 to 100 nm, and the nanowires orthogonally intercrossed with each other to form 3D nanowire networks.

The structural changes of the prepared nanowires with the increase in the introduced oxygen flow rate had also been investigated using the XRD patterns. As shown in Fig. 3, the crystal structures of the products could be well indexed to monoclinic WO_2 (JCPDS card: no. 05-0431), monoclinic $W_{18}O_{49}$ (JCPDS card: no. 36-0101), and monoclinic WO_3 (JCPDS card: no. 43-1035) in sequence with the increase in the oxygen flow rate from 0 to 1.5 sccm. However, when the oxygen flow rate increased to 1.5 sccm, although all the diffraction peaks could be well indexed to monoclinic WO_3, the intensity of the peak assigned to the diffraction peak from the (002) plane was much stronger than the ones from the (020) and (200) planes, which was inconsistent with the standard JCPDS card of monoclinic WO_3 in which three peaks from the (002), (020) and (200) planes had almost the same intensities. This may be due to the preferred orientation along the [002] direction during the growth of 3D-WO_3 nanowire networks, making them different from the cubic structure WO_3 nanowire network reported by Zhou *et al.*[26]

In order to further confirm the structure of 3D-WO_3 nanowire networks and to reveal their growth mechanism, we varied the evaporation time to record the growth process. As demonstrated in Fig. 4, the typical cross-sectional SEM images show that the nanorods with larger diameters in the range of 200–500 nm firstly grew on the bottom layer (as shown in Fig. 4(b)), and then the nanorods became smaller in diameter and generated some branches to form tree-like nanostructures (denoted as nanotrees) on the middle layer (as shown in Fig. 4(c)). With the increase in evaporation time, the stems of the nanotrees further became smaller, and simultaneously the branches generated secondary branches. These secondary branches crossed over with each other to form three-dimensional nanowire networks at the top layer (as shown in Fig. 4(d)). Since the diameter of the nanotree stems had decreased close to the size of the secondary branches, no obvious stems in the network can be distinguished if one looks at the network from the top-view SEM image (*e.g.*, Fig. 2(f)). The nanorods, nanotrees, and nanowire networks were found to be formed at the evaporation time of 1, 5 and 20 minutes in our experiments, respectively. The XRD spectra of the samples prepared under the corresponding evaporation time are shown in the left panel of Fig. 5, and their SEM images are also shown in the right panel of Fig. 5. Besides the characteristic peaks from silicon substrates which are indicated by small black squares, all the diffraction peaks in each XRD spectrum can be indexed to the WO_3 monoclinic structure. It means that the nanostructures with high crystallinity had been synthesized even at the beginning of the evaporation. Notably, compared with the diffraction peaks from the (020) and (200) planes, the intensity of the peak from the (002) plane increased as the evaporation time increased from 1 to 20 minutes, and finally became much stronger than the other peaks. Since the nanotrees and nanowire networks were formed at the later period of the crystal growth, it is reasonable to believe that preferred orientation growth occurred during the formation of the nanotrees and nanowire networks, in which the nanostructures with their (002) planes parallel to the substrate could preferentially grow and the others could be suppressed. Based on these results, the occurrence of the preferred orientation growth along the [002] direction will be discussed in the latter part of this section.

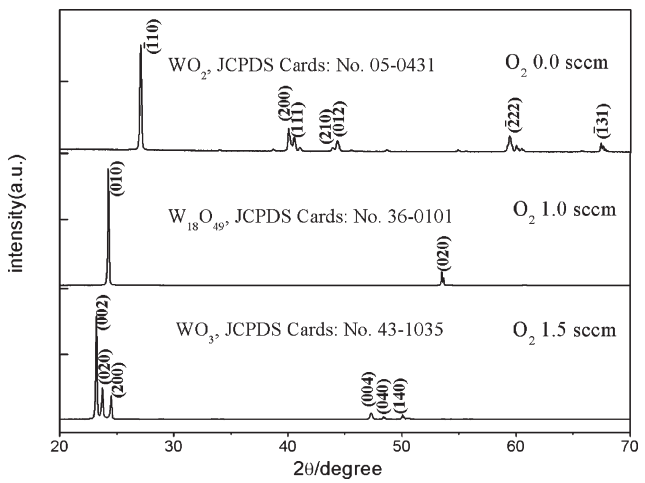

Fig. 3 XRD spectra for the products prepared at oxygen flow rates of 0.0, 1.0, and 1.5 sccm. The samples are fabricated on quartz substrates.

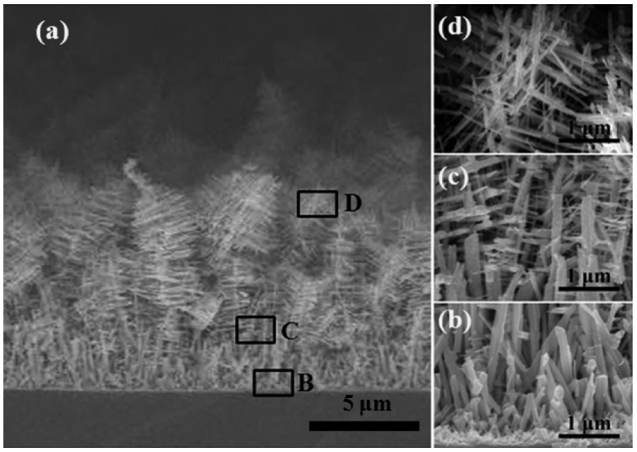

Fig. 4 (a) Typical cross-sectional SEM image of 3D-WO_3 nanowire networks on the silicon substrates. (b–d) High-magnification SEM images of regions B, C, and D in (a).

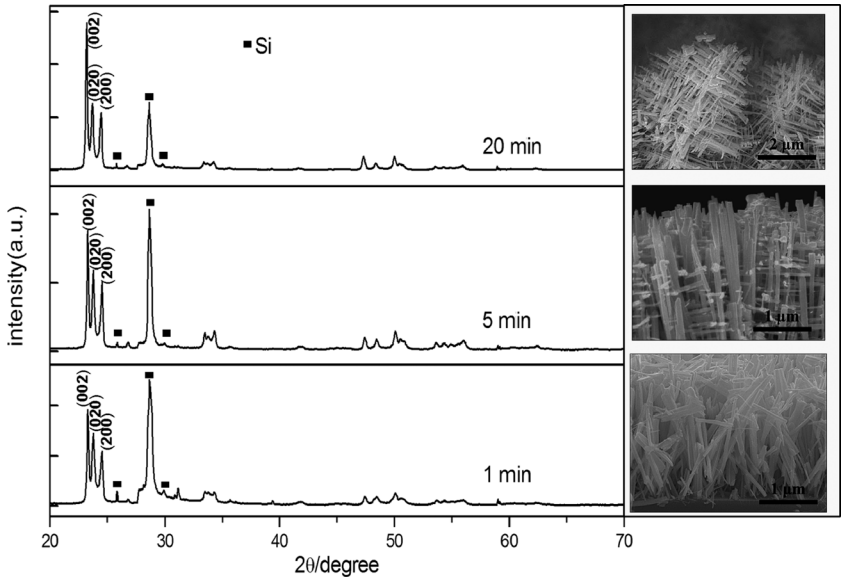

Fig. 5 XRD spectra (left panel) and SEM images (right panel) of 3D-WO_3 nanowire networks prepared under the evaporation time of 1, 5, and 20 min, respectively. The diffraction peaks from silicon substrates are indicated by small black squares.

The preferred orientation growth along the direction of [002] in 3D-WO_3 nanowire networks had also been proven in the high-resolution transmission electron microscopy (HRTEM). The typical TEM image in Fig. 6(a) shows a broken WO_3 nanowire network segment with several junctions, and the broken fractures of the secondary branches are indicated by the hollow arrowheads. The angle of the junctions nearly equaled 90°, which was consistent with the WO_3 monoclinic structure at room temperature with the following lattice constants: α = 90°, β = 90.91°, and γ = 90° (JCPDS card: no. 43-1035). Selected-area electron diffraction (SAED) patterns as shown in Fig. 6(b–d) were recorded from regions B, C, and D in Fig. 6(a), proving that the entire network was single crystalline. It is noticeable that there were streaks in the SAED patterns and these streaks were normal to the growth direction of the nanowires, as indicated by the white arrowheads in Fig. 6(b–d). These streaks could arise from the presence of planar oxygen vacancies parallel to the growth direction, which had been proven by Zhou *et al.*,[26] and thus the presence of planar defects was likely responsible for the branch growth during the formation of nanotrees and nanowire networks. The main stem of networks in the nanowire network segment grew along the [002] direction, which was confirmed by its HRTEM image in the inset of Fig. 6(a). The HRTEM image clearly shows that the inter-planar spaces along the [002] and [020] directions were 0.384 and 0.377 nm, respectively, which agreed with the XRD results. This revealed that the stems of nanotrees or nanowire networks grew along the [002] direction, and stood up on the substrate, resulting in the enhancement of the diffraction peak from the (002) plane in XRD.

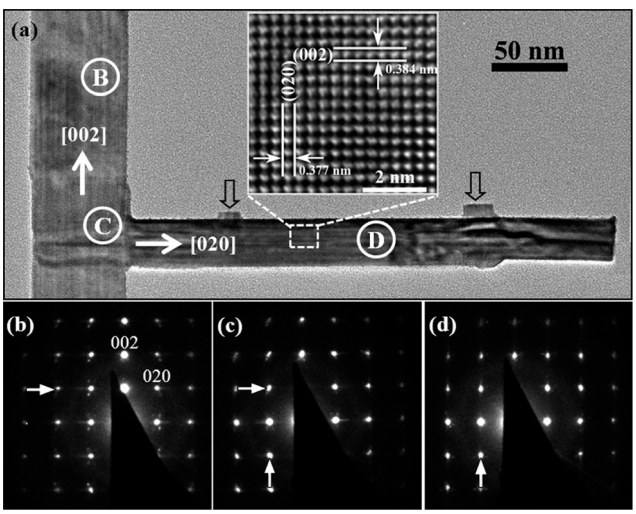

Fig. 6 (a) TEM image of a WO_3 nanowire network segment (the hollow arrowheads indicate the positions of fractures). Inset: HRTEM image of the white-dashed-square region in (a). (b–d) SAED patterns of regions B, C, and D in (a). Streaks in the SAED patterns are marked by the white arrowheads.

The question arises as to what is the growth process responsible for the formation of 3D-WO_3 nanowire networks. The synthesis process was a thermal evaporation process without any catalyst, and thus the vapor–solid (VS) growth process should be the dominating mechanism in this case.[29] Tungsten powder (which was used as a source) with a melting point of more than 3000 °C could not be gasified at the peak temperature of 1100 °C in our synthesis process, and thus the vapor in the VS growth model should be tungsten oxide vapor and not tungsten vapor. As shown in Fig. 1(b), the surface layer of tungsten particles could be oxidized by the residual oxygen in the chamber or the introduced oxygen into tungsten oxide, and then the solid tungsten oxide could be evaporated into tungsten oxide vapor at the peak temperature. The newly exposed tungsten on the particle surface

could also be oxidized into tungsten oxide and then become tungsten oxide vapor. Therefore, the introduced oxygen should be a key factor to synthesize the tungsten oxide nanostructures, which determined the evaporation speeds and the rates of W and O in the products. Since the nanorods were fabricated without the introduced oxygen as demonstrated in the results shown in Fig. 2(a and b), the vapor source in the VS growth model in this case should come from a thin tungsten oxide layer which had been formed on tungsten particle surfaces in air or under low vacuum conditions (about 10 Pa in our experiments) during the evaporation. In order to distinguish this, XRD was applied to analyze whether the tungsten powder had been oxidized in air before evaporation. As shown in Fig. S1 in the ESI,† all diffraction peaks agreed with the elemental tungsten phase (JCPDS card: no. 04-0806), and no obvious diffraction peak which came from tungsten oxide was observed. However, for fine W particles, a thin surface oxide layer is easily formed in air, which could not crystallize well and cannot give enough information regarding the existence of the oxide layer in the XRD test. Thus, this XRD result cannot exclude the fact that the tungsten oxide layer was not formed in air, but the W particles should be further oxidized by the residual oxygen in the chamber during the temperature rise period of the thermal evaporation to form the oxide layer.

Based on all the experimental and analysis findings above, the growth process for the formation of 3D-WO_3 nanowire networks was proposed as shown in Fig. 7, described as follows: (1) firstly, as the evaporation started, the thin tungsten oxide layer could easily turn into vapor, and be deposited on the surface of the substrate to form WO_2 nanorods. (2) Then, the introduced pure oxygen gas should play two roles. One role is to further oxidize WO_2 nanorods into WO_3 nanorods on the substrate, and the other role is to regenerate tungsten oxide on tungsten particle surfaces in the tungsten boat. Since the diameters of nanorods or nanowires which grew at later stages became smaller and smaller with evaporation, it sounds very reasonable to believe that the regeneration speed of tungsten oxide was lower than the gasification speed. Therefore, the evaporation speed was totally determined by the regeneration speed of tungsten oxide on the source particles. (3) As the introduced oxygen flow rate increased, the evaporation speed was accelerated to be so fast that the newly grown tungsten oxide nanowires on the substrate were not further oxidized into WO_3 in time, resulting in the presence of planar oxygen vacancies in the body of nanowires. These planar oxygen vacancies could induce nanowires to grow along different directions and to form nanotrees. (4) The branches of nanotrees also generated secondary branches with the evaporation time, and the secondary branches crossed over with each other to form nanowire networks at the last stage of the crystal growth. These nanowire networks were likely to form on top of the upstanding nanotrees as shown in the cross-sectional SEM images in Fig. 4, which could be attributed to the obstructing effect of these upstanding nanotrees on the further growth of nanotrees in other directions. The competition of growth space between nanostructures rather happened in the transverse direction than in the longitudinal direction. Thus, the upstanding nanotrees could further grow into the nanowire network along the longitudinal direction, and the growth of nanowire network along the other directions could be suppressed. This could be applied to explain why a preferred orientation growth just occurred during the formation of nanowires and nanowire networks, in which the upstanding nanorods with their (002) planes parallel to the substrate could preferentially grow into nanotrees and nanowire networks, compared with the others.

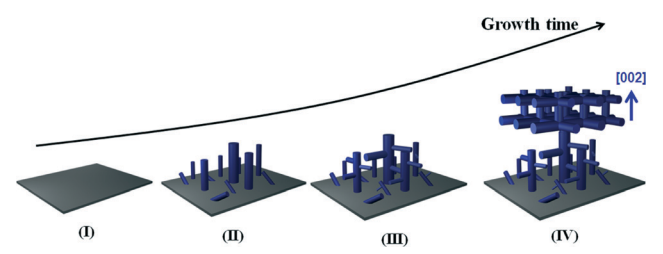

Fig. 7 The growth process proposed for the formation of 3D-WO_3 nanowire networks (see text for details).

Conclusions

In summary, different morphologies, single-crystalline tungsten oxide nanorods or nanowires have been fabricated by controlling the introduced oxygen flow rate in a one-step high temperature, catalyst free, thermal evaporation deposition process. The formation process of complex three-dimensional tungsten oxide nanowire networks was recorded by SEM: under oxygen-rich growth conditions, tungsten oxide nanorods firstly grew on the substrates, and then the nanorods generated some branches to form nanotree structures with the increase in evaporation time. The stems of nanotrees became smaller, and simultaneously the branches generated secondary branches; these secondary branches crossed over with each other to form three-dimensional nanowire networks on top of the nanotrees. A preferred orientation growth and a planar-defect-induced growth are observed in XRD and HRTEM, and they are also responsible for the formation of complex nanowire networks. A detailed growth process for the formation of complex 3D-WO_3 nanowire networks is given in this paper, which may be useful to investigate controllable synthesis of three-dimensional metal oxide nanowire networks. Furthermore, the newly grown special nanostructures, which are composed of nanorods, nanotrees, and nanowire networks from the bottom to the top, should be the foundation for investigating the applications of tungsten oxide in electrochromics/gasochromics, gas sensors, and photocatalysis, and the related electronic or optoelectronic devices.

Acknowledgements

The authors gratefully acknowledge the financial support of the projects from the National Natural Science Foundation of

China (no. 51402218, 61108091, and 61307026), Guangdong University Talent Introduction of Special Funds (no. Yue Cai-Jiao [2011]431), Science Foundation for Young Teachers of Wuyi University (Nos. 2013zk05, 2014td01) and the Open Fund of Guangdong High Education Research Center of Light Chemical Cleaner Production Engineering Technology.

References

1 C. G. Granqvist, *Nat. Mater.*, 2006, **5**, 89–90.
2 V. Wittwer, M. Datz, J. Ell, A. Georg, W. Graf and G. Walze, *Sol. Energy Mater. Sol. Cells*, 2004, **84**, 305–314.
3 Y. He and Y. Zhao, *J. Phys. Chem. C*, 2008, **112**, 61–68.
4 S. K. Deb, *Sol. Energy Mater. Sol. Cells*, 2008, **92**, 245–258.
5 K. Shimizu, I. Chinzei, H. Nishiyama, S. Kakimoto, S. Sugaya, H. Yokoi and A. Satsuma, *Sens. Actuators, B*, 2008, **134**, 618–624.
6 C. H. Hsu, C. C. Chang, C. M. Tseng, C. C. Chan, W. H. Chao, Y. R. Wu, M. H. Wen, Y. T. Hsieh, Y. C. Wang, C. L. Chen, M. J. Wang and M. K. Wu, *Sens. Actuators, B*, 2013, **186**, 193–198.
7 R. Abe, H. Takami, N. Murakami and B. Ohtani, *J. Am. Chem. Soc.*, 2008, **130**, 7780–7781.
8 M. Grätzel, *Nature*, 2001, **414**, 338–344.
9 C. Santato, M. Ulmann and J. Augustynski, *Adv. Mater.*, 2001, **13**(7), 511–514.
10 P. Yang, Y. Li, Z. Lin, Y. Ding, S. Yue, C. P. Wong, X. Cai, S. Tan and W. Mai, *J. Mater. Chem. A*, 2014, **2**, 595–599.
11 J. Y. Luo, W. Li, F. Chen, X. X. Chen, W. Da Li, H. Y. Wu, Y. J. Gao and Q. G. Zeng, *Sens. Actuators, B*, 2014, **197**, 81–86.
12 J. Y. Luo, X. X. Chen, W. D. Li, W. Y. Deng, W. Li, H. Y. Wu, L. F. Zhu and Q. G. Zeng, *Appl. Phys. Lett.*, 2013, **102**, 113104.
13 J. W. Liu, J. L. Wang, J. Xu, H. H. Li and S. H. Yu, *Nano Lett.*, 2013, **13**, 3589–3593.
14 Y. C. Her and C. C. Chang, *CrystEngComm*, 2014, **16**, 5379–5386.
15 Z. G. Zhao and M. Miyauchi, *Angew. Chem., Int. Ed.*, 2008, **47**, 7051–7055.
16 F. Wang, Y. Wang, X. Zhan, M. Safdar, J. Gong and J. He, *CrystEngComm*, 2014, **16**, 1389–1394.
17 N. Barson and U. Weimar, *J. Electroceram.*, 2001, **7**, 143–167.
18 L. F. Zhu, J. C. She, J. Y. Luo, S. Z. Deng, J. Chen, X. W. Ji and N. S. Xu, *Sens. Actuators, B*, 2011, **153**, 354–360.
19 Y. Huang, X. F. Duan, Q. Wei and C. M. Lieber, *Science*, 2001, **291**, 630–633.
20 D. Whang, S. Jin, Y. Wu and C. M. Lieber, *Nano Lett.*, 2003, **3**, 1255–1259.
21 Z. W. Pan, S. M. Mahurin, S. Dai and D. H. Lowndes, *Nano Lett.*, 2005, **5**, 723–727.
22 M. McCune, W. Zhang and Y. Deng, *Nano Lett.*, 2012, **12**, 3656–3662.
23 W. Wang, M. Tian, A. Abdulagatov, S. M. George, Y. C. Lee and R. Yang, *Nano Lett.*, 2012, **12**, 655–660.
24 Z. Gu, F. Liu, J. Y. Howe, M. P. Paranthaman and Z. Pan, *Cryst. Growth Des.*, 2009, **9**, 35–39.
25 Y. Q. Zhu, W. Hu, W. K. Hsu, M. Terrones, N. Grobert, J. P. Hare, H. W. Kroto, D. R. M. Walton and H. Terrones, *Chem. Phys. Lett.*, 1999, **309**, 327–334.
26 J. Zhou, Y. Ding, S. Z. Deng, L. Gong, N. S. Xu and Z. L. Wang, *Adv. Mater.*, 2005, **17**, 2107–2110.
27 Y. Zhang, Y. Chen, H. Liu, Y. Zhou, R. Li, M. Cai and X. Sun, *J. Phys. Chem. C*, 2009, **113**, 1746–1750.
28 H. J. Chen, N. S. Xu, S. Z. Deng, D. Y. Lu, Z. L. Li, J. Zhou and J. Chen, *Nanotechnology*, 2007, **18**, 205701.
29 Z. W. Pan, Z. R. Dai and Z. L. Wang, *Science*, 2001, **291**, 1947–1949.

